Breathing dynamics of symmetry-broken temporal cavity solitons in Kerr ring resonators

Gang Xu, Lewis Hill, Gian-Luca Oppo, Miro Erkintalo, Stuart Murdoch, Stéphane Coen, Julien Fatome

Breathing dynamics of symmetry-broken temporal cavity solitons in Kerr ring resonators

GANG XU[1,2,*], LEWIS HILL[3,4,5,*], JULIEN FATOME[1,2,6], GIAN-LUCA OPPO[3], MIRO ERKINTALO[1,2], STUART G. MURDOCH[1,2], AND STÉPHANE COEN[1,2]

[1] Physics Department, The University of Auckland, Private Bag 92019, Auckland 1142, New Zealand
[2] The Dodd-Walls Centre for Photonic and Quantum Technologies, New Zealand
[3] SUPA and Department of Physics, University of Strathclyde, Glasgow G4 0NG, Scotland, EU
[4] National Physical Laboratory, Hampton Road, Teddington, TW11 0LW, UK
[5] Max Planck Institute for the Science of Light, 91058 Erlangen, Germany
[6] ICB, UMR 6303 CNRS, Université Bourgogne-Franche-Comté, 9 Av. Alain Savary, BP 47870, F-21078 Dijon, France
[*] Corresponding authors: gang.xu@auckland.ac.nz, lewis.hill@strath.ac.uk. G.X. and L.H. contributed equally to this work.

We investigate theoretically and experimentally the instabilities of symmetry-broken, vectorial, bright cavity solitons of two-mode nonlinear passive Kerr resonators. Through comprehensive theoretical analyses of coupled Lugiato-Lefever equations, we identify two different breathing regimes where the two components of the vectorial cavity solitons breathe respectively in-phase and out-of-phase. Moreover, we find that deep out-of-phase breathing can lead to intermittent self-switching of the two components, spontaneously transforming a soliton into its mirror-symmetric state. In this process, solitons are also sometimes observed to decay. All our theoretical predictions are confirmed in experiments performed in an optical fiber ring resonator, where cavity soliton symmetry breaking occurs across the polarization modes of the resonator. To the best of our knowledge, our study constitutes the first experimental report of breathing instabilities of multi-component optical solitons of driven nonlinear resonators.

Breathing or pulsating solitons are nonlinear waves in which energy is localized in space but oscillates in time, or vice versa. They are fundamental features of soliton theory and arise through various mechanisms. In conservative systems, they are found, e.g., in hydrodynamics [1], Bose-Einstein condensates (BEC) [2, 3], as well as nonlinear optics [4–6]. In the dissipative context, they have been observed in systems such as gas discharges [7] and more recently in passive driven scalar Kerr resonators [8] and mode-locked lasers [9].

So far experimental realizations of breathing solitons have been mostly concerned with scalar, single component solitons. While a handful of theoretical studies have highlighted that multi-component (vector) solitons can also have associated breathing states [10–12], experimental results have been limited, and restricted to fiber lasers [13, 14]. In this Letter, we report experimental observations of breathing states associated with two-component dissipative optical solitons in coherently-driven passive Kerr resonators. Dissipative solitons of such systems manifest themselves in the form of temporal cavity solitons (CSs) [15]: ultra-short light pulses that can persist indefinitely in the resonator. Such CSs play a key role in the generation of microresonator Kerr frequency combs [16]. While most studies have focussed on scalar (or quasi-scalar) CSs, recent observations performed in isotropic optical fiber resonators with two equally-driven polarization modes have highlighted the existence of vector CS solutions [17] arising through a spontaneous symmetry breaking (SSB) instability. Here, the solitons comprise two orthogonally-polarized, temporally localized, bright components of different amplitudes. By symmetry, these CS states always come in pairs that are mirror images of each other, i.e., where the two polarization components — dominant and depressed — are interchanged. We analyse in detail, numerically and experimentally, the dynamic instabilities of these new symmetry broken CSs. Compared to scalar CSs [8], they exhibit more complex oscillating dynamics: the two components can oscillate either in-phase or out-of-phase, and deep polarization fluctuations can randomly induce spontaneous switching between the two mirror-like states. Our work highlights a novel range of instabilities of vector CSs, and could have relevance for applications such as frequency comb generation.

We start with theoretical considerations. The solitons under interest are described by the following normalized coupled Lugiato Lefever equations (LLEs) [17],

$$\frac{\partial E_{1,2}(t,\tau)}{\partial t} = \left[-1 + i(|E_{1,2}|^2 + B|E_{2,1}|^2 - \Delta) + i\frac{\partial^2}{\partial \tau^2}\right] E_{1,2} + S \quad (1)$$

where subscripts 1 and 2 refer to the two orthogonal polarization modes of the resonator. t is a slow time variable that describes the evolution of the modal field envelopes $E_{1,2}$ on the scale of the cavity photon lifetime, while τ is a fast time that describes the temporal profile of these envelopes over a single roundtrip. Terms on the right hand side of Eqs. (1) represent, respectively, cavity loss, self- and cross-phase modulation (XPM,

with coefficient B), the detuning between the driving laser frequency and the closest cavity resonance, chromatic dispersion (here taken anomalous), and driving. For this study, we consider an isotropic resonator where the two modes are equally driven: the detuning Δ and driving amplitude S are the same for both modes. Consequently, the above equations satisfy an interchange symmetry, $E_1 \rightleftarrows E_2$.

The *homogenous* steady state (HSS) solutions of Eqs. (1), for which $\partial E_{1,2}/\partial t = \partial E_{1,2}/\partial \tau = 0$, have been known for some time to exhibit SSB [18, 19]. Much work has been completed recently observing this HSS symmetry breaking, and analyzing its characteristics, stability and dynamics for a variety of parameters [20–22]. In particular, experiments performed with two counter-propagating beams in a Kerr microresonator have revealed oscillatory instabilities as well as self-switching between the two asymmetric HSS solutions [23]. These switching dynamics were shown to be either chaotic or periodic, depending on cavity detuning. Our present study remarkably shows that symmetry-broken CSs exhibit similar behavior.

Figures 1(a)–(b) show two representative examples of dynamical behaviors of two-component symmetry-broken CSs. These were obtained by numerical integration of Eqs. (1) using $S = 2.1$ and $B = 1.6$ (these parameters are chosen to match the experiments presented below) and different detunings Δ as indicated. In each case, we plot the temporal intensity profiles of the two

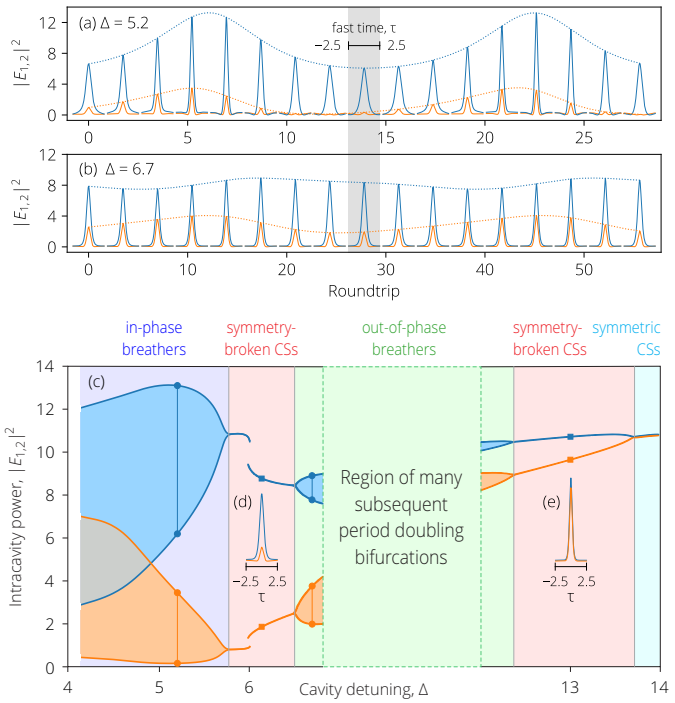

Fig. 1. Numerical examples of (a) in-phase and (b) out-of-phase symmetry-broken CS breathers. Solid curves are temporal intensity profiles of the two polarization components at selected roundtrips; dotted lines connect peak power levels. (c) Maxima and minima of the peak power levels of the dominant (blue) and depressed (orange) components versus detuning Δ. Shading in between the curves indicate the oscillation range of breathers. Background colors identity different dynamical regimes (see text). Insets (d) and (e) show the fixed profiles of stationary CSs for $\Delta = 6.1$ and 13, respectively [same vertical scale as (a), (b)]. $S = 2.1$ and $B = 1.6$ for all panels.

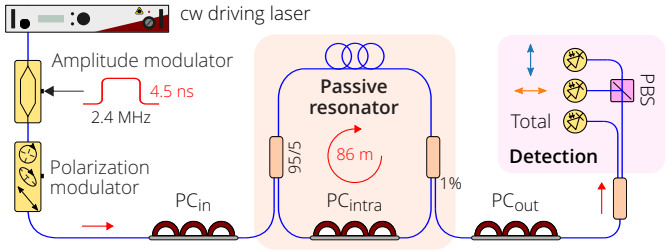

Fig. 2. Simplified diagram of the experimental setup. PC: polarization controller; PBS: polarization beam splitter.

polarization components (blue and orange, solid), $|E_{1,2}|^2$ versus fast time τ, at selected roundtrips. The dotted lines connect the peak power levels. Here the field E_1 (blue) is dominant while E_2 (orange) is depressed, but the mirror solution where E_1 and E_2 are interchanged also exists. In (a), for the low detuning value, the two components breathe nearly in-phase, while the dynamics exhibit more an out-of-phase character for the large detuning example (b). This qualitative and quantitative dependence of the breather dynamics on the detuning is explored further in Fig. 1(c), which provides an overview of how the different dynamical regimes are organized over a wider range of detunings. The solid curves depict the extrema of the normalized peak power of the breathing oscillations of the dominant (blue) and depressed (orange) components of the CS. The shading between these curves indicates the oscillation range during breathing (overlap in grey); the round markers joined by vertical lines correspond to Figs. 1(a)–(b). The shaded background colors highlight the different dynamical behaviors. We observe that the parameter range for in-phase and out-of-phase CS breathers are quite distinct. In-phase CS breathers appear at low detuning (light-blue/purple region) through a Hopf instability, in a way reminiscent of *scalar* breather CSs previously reported in optical fiber rings and in microresonators [8, 24]. CSs cease to exist left of that region. Out-of-phase CS breathers are found at higher detuning (green area) in between two opposite Hopf bifurcations. Here the CS breathers can undergo complex period-doubling bifurcations, as well as deep breathing characterized by self-switching dynamics of the two polarization components [23]. This switching can be chaotic or, for some narrow ranges of parameters, periodic. For lower values of S, these dynam-ics get progressively simpler as the green region shrinks and eventually closes. Out-of-phase CS breathers are bracketed on both sides by *stationary* symmetry-broken CSs (light-red region), with two examples of (fixed) intensity profiles shown in insets (d) and (e) [with matching square markers]. Finally, *symmetric* ($E_1 = E_2$) stationary CSs also exist on the high detuning side (cyan region on the far right). The transition from symmetric to symmetry-broken CSs through SSB is described in Ref. [17].

To test the numerical predictions of Fig. 1, we used the same experimental configuration as in Ref. [17] (see Fig. 2 for a simplified diagram). The setup consists of an 86 m-long optical fiber ring resonator made up of standard single-mode fiber. The XPM coefficient B was measured at 1.58 [22]. The cavity includes a 95/5 coupler for injection of the driving field and a 1 % tap coupler to extract the intracavity field for analysis. Overall, the resonator presents a free spectral range (FSR) of 2.39 MHz and a finesse of about 42. The cavity is synchronously driven with 4.5 ns-long flat-top pulses carved into a 1 kHz-linewidth continuous-wave 1.55 µm-wavelength laser by an amplitude

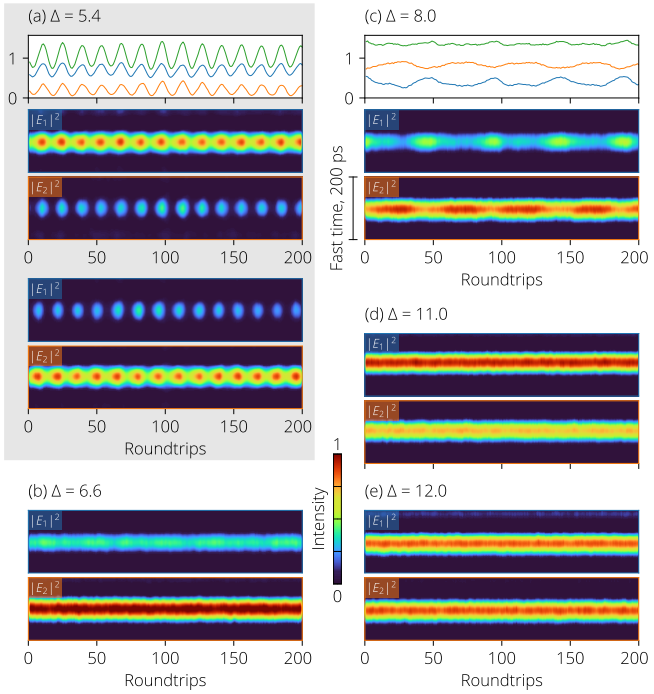

Fig. 3. Pairs of pseudo-color plots are horizontal concatenations of measured temporal intensity profiles (over 200 ps of fast time) of the two polarization components of CSs at the cavity output for 200 subsequent roundtrips ($S = 2.1$). When present on top, line plots show corresponding evolution of the two components (blue and orange) at the pulse center, as well as total intensity (green). (a) $\Delta = 5.4$, in-phase symmetry-broken CS breathers; the two mirror states are shown separately. (b) and (d), respectively $\Delta = 6.6$ and 11, stationary symmetry-broken CSs. (c) $\Delta = 8$, out-of-phase symmetry-broken CS breathers. (e) $\Delta = 12$, stationary symmetric CS.

modulator. The laser frequency is actively locked at a set detuning from a cavity resonance as described in [25]. Polarization is managed through three polarization controllers (PC). An intracavity PC (PC_{intra}) is used to achieve effective isotropy between the two polarization modes of the resonator using the technique of Ref. [22]. Note that this technique makes coherent coupling terms average to zero, ensuring the validity of Eqs. (1). Another controller placed before the input coupler (PC_{in}) is set to project the input state of polarization (SOP) equally onto the two cavity modes to realize balanced driving conditions. This balance is actively controlled by a feedback loop (not shown) acting on a polarization modulator placed in the path of the driving beam for stabilization against environmental perturbations. Together with cavity isotropy, this guarantees the exchange symmetry between the two modes, enabling SSB. Finally, a third PC is placed at the output (PC_{out}) in front of a polarization beam-splitter (PBS) so that we can monitor the intensities of the two polarization modes through individual 10 GHz-bandwidth photodiodes [22]. The total output intensity is also measured separately.

The experiment was run with 700 mW of peak driving power, corresponding to a normalized driving strength $S = 2.1$ as in the simulation results presented in Fig. 1. For various values of cavity detuning, we excited temporal CSs through mechanical perturbation and then recorded with an ultra-fast 40 GSa/s real-time oscilloscope their temporal intensity profiles (individual polarization components and total intensity) at the cavity output over subsequent roundtrips. A first set of data is presented in Fig. 3. Here pairs of pseudo-color plots are made up of horizontal concatenations of such profiles (fast time versus roundtrip number) for the two orthogonal polarization components. Line plots on top (when present) show the corresponding intensities at the center of the CS (blue and orange), while the green curve is the total intensity at the same location. In Fig. 3(a), $\Delta = 5.4$, we report observation of symmetry-broken *in-phase* temporal CS breathers. The two polarization components have markedly different intensity levels, yet oscillate synchronously with a period of about 15 cavity roundtrips. The in-phase nature of the breathing is highlighted by the deep oscillations in the total intensity (green curve on top). Here, both mirror states are shown in separate pairs of pseudo-color plots. As can be seen, the overall symmetry is excellent, and the two states clearly display identical behaviors and characteristics (although not shown, we have been able to observe mirror states of all the cases discussed in this Letter). When the detuning is increased to $\Delta = 6.6$, Fig. 3(b), the CSs stabilize: no breathing is discernible, although the symmetry remains broken (different intensity levels for the two polarization components). This case corresponds to stationary symmetry-broken CSs already reported in [17]. Increasing the detuning further, to $\Delta = 8$, Fig. 3(c), reveals a different instability regime characterized by symmetry-broken *out-of-phase* temporal CS breathers. Here the total intensity is near constant, and the oscillation period is much longer, about 50 roundtrips, in comparison to the in-phase breathers in (a). We should note that the breather evolution in Fig. 3(c) does not appear to be strictly periodic. In fact, a number of distinct aperiodic and chaotic behaviors exist in this region of parameter space, and periodic oscillations are only observed occasionally, making the latter very sensitive to environmental fluctuations. Past the region of out-of-phase CS breathers, we recover stationary symmetry-broken CSs, Fig. 3(d), $\Delta = 11$ [same behavior as in Fig. 3(b)]. The symmetry of these CSs is eventually restored for even larger values of the detuning, $\Delta = 12$, Fig. 3(e). Here we have left the SSB region [17]. CSs cease to exist altogether with further increase in the detuning. Overall the observed dynamics are in very good qualitative agreement with the phase portrait of Fig. 1(c), though we note that the precise values of detunings of each dynamical region do not always agree between simulations (Fig. 1) and experiment. We attribute this fact to the sensitivity of the breathing regimes to the exact parameter values as well as uncertainties and experimental imperfections, such as a small desynchronization of the pulsed driving.

We now illustrate in more detail the more complex dynamics that out-of-phase CS breathers can exhibit. For some particular values of the detuning Δ, the solitons breathe irregularly, as already mentioned above, and sometime with such high contrast that a spontaneous switching of the two polarization components may occur. One such self-switching event is illustrated in Figs. 4(a)–(d) for a detuning value $\Delta = 8.2$ [and the same driving power as in Fig. 3]. Pseudo-color plots (a)–(c) show the evolution against roundtrip number of the temporal intensity profiles of, respectively, the two polarization components as well as the total intensity (halved) of an out-of-phase CS breather, while panel (d) highlights the dynamics at the center of the pulse. The dominant and depressed components self-switch around roundtrip number 350, turning the breather into its mirror state. Breathing oscillations are clearly visible on the two polarization components before and after the switch, and their out-of-phase nature correlates with the near constant total intensity observed

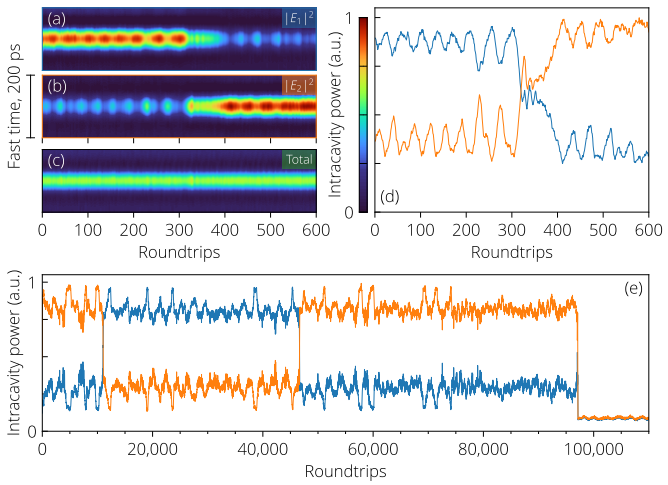

Fig. 4. Self-switching of out-of-phase symmetry-broken CS breathers. (a)-(c) Roundtrip-by-roundtrip evolution of measured temporal intensity profiles of (a), (b) individual polarization components — with corresponding line plots (blue and orange) at the pulse center in (d) — and (c) total intensity (halved); $\Delta = 8.2$, $S = 2.1$. (e) Long term evolution of the two polarization components showing two self-switching events, followed by a decay of the CS breather; $\Delta = 8.4$, $S = 2.1$.

in Fig. 4(c). We must insist that, as has been observed with HSSs [23], the switch we report in Figs. 4(a)–(d) occurs *spontaneously*; this contrasts with the switching of stationary symmetry-broken CSs reported in [17] and for which an external perturbation was required. Self-switching dynamics of incoherent vector solitons has also been reported in fiber lasers [26].

Simulations indicate that self-switching of out-of-phase CS breathers can in principle occur periodically. However, this periodicity only exists in such narrow parameter ranges that we have been unable to observe it in practice because of experimental fluctuations. Rather, we have observed the much more common (according to simulations) behavior where the breathers self-switch at random intervals. An example of multiple self-switching is presented in Fig. 4(e) [same representation as (d)]. Two successive self-switching events are clearly visible, separated by about 36,000 roundtrips (or ~ 15 ms). This interval is much longer than the breathing period itself (which is about 40 roundtrips here). We note that, in these measurements, the pulses are only sampled every 7 roundtrips (because of the limited memory depth of the oscilloscope); as a result, the actual breathing is not very well resolved. In Fig. 4(e), the CS breather attempts a third self-switch at about roundtrip number 97,000, but this switching attempt imparts such a strong perturbation to the breather that it leads to its decay. The system then ends up in the lower HSS of the bistable response. A decay of the CS after a small number of self-switching is the typical scenario in this parameter range, as also confirmed by numerical simulations.

In summary, we studied theoretically and experimentally the dynamical instabilities of symmetry-broken bright CSs of two-mode driven passive Kerr resonators. To the best of our knowledge, our work constitutes the first experimental observations of multi-component breather solitons in a driven resonator. Our experiments were performed using the two co-propagating polarization modes of an isotropic optical fiber ring resonator. We have identified two different breathing regimes, dependent on the cavity detuning, where the components of the CSs can oscillate either in-phase or out-of-phase. The out-of-phase CS breathers can further exhibit more complex dynamics that can lead to spontaneous self-switching of the dominant and depressed components of the solitons, or to their decay. Our investigations pave the way to a more complete understanding of the complexities of dissipative vector solitons.

Funding Information. Royal Society Te Apārangi (New Zealand) Marsden Fund (18-UOA-310) and Rutherford Discovery Fellowship (for ME, 15-UOA-015); CNRS International Project WALL-IN. **Acknowledgements.** LH and GLO thank the financial support from the Mac Robertson Trust, the Dodd Walls Centre, EPSRC DTA (EP/M506643/1), and NPL. **Disclosures.** The authors declare no conflicts of interest. **Data availability.** The data that support the findings of this study are available from the corresponding author upon reasonable request.

REFERENCES

1. A. Chabchoub, N. P. Hoffmann, and N. Akhmediev, Phys. Rev. Lett. **106**, 204502 (2011).
2. S.-W. Su, S.-C. Gou, I.-K. Liu, A. S. Bradley, O. Fialko, and J. Brand, Phys. Rev. A **91**, 023631 (2015).
3. J. Yang, SIAM J. Appl. Math. **76**, 598 (2016).
4. I. V. Barashenkov, D. E. Pelinovsky, and E. V. Zemlyanaya, Phys. Rev. Lett. **80**, 5117 (1998).
5. A. De Rossi, C. Conti, and S. Trillo, Phys. Rev. Lett. **81**, 85 (1998).
6. B. Kibler, J. Fatome, C. Finot, G. Millot, F. Dias, G. Genty, N. Akhmediev, and J. M. Dudley, Nat. Phys. **6**, 790 (2010).
7. I. Müller, E. Ammelt, and H.-G. Purwins, Phys. Rev. Lett. **82**, 3428 (1999).
8. F. Leo, L. Gelens, Ph. Emplit, M. Haelterman, and S. Coen, Opt. Express **21**, 9180 (2013).
9. J. Peng, S. Boscolo, Z. Zhao, and H. Zeng, Sci. Adv. **5**, eaax1110 (2019).
10. D. Michaelis, U. Peschel, C. Etrich, and F. Lederer, IEEE J. Quantum Electron. **39**, 255 (2003).
11. N. Vishnu Priya, M. Senthilvelan, and M. Lakshmanan, Phys. Rev. E **88**, 022918 (2013).
12. Y.-Q. Yao, W. Han, J. Li, and W.-M. Liu, J. Phys. B: At. Mol. Opt. Phys. **51**, 105001 (2018).
13. Y. Luo, Y. Xiang, P. P. Shum, Y. Liu, R. Xia, W. Ni, H. Q. Lam, Q. Sun, and X. Tang, Opt. Express **28**, 4216 (2020).
14. W. Du, H. Li, J. Li, Z. Wang, Z. Zhang, S. Zhang, and Y. Liu, Opt. Express **29**, 14101 (2021).
15. F. Leo, S. Coen, P. Kockaert, S.-P. Gorza, Ph. Emplit, and M. Haelterman, Nat. Photon. **4**, 471 (2010).
16. S. Coen, H. G. Randle, T. Sylvestre, and M. Erkintalo, Opt. Lett. **38**, 37 (2013).
17. G. Xu, A. U. Nielsen, B. Garbin, L. Hill, G.-L. Oppo, J. Fatome, S. G. Murdoch, S. Coen, and M. Erkintalo, Nat. Commun. **12**, 4023 (2021).
18. A. E. Kaplan and P. Meystre, Opt. Commun. **40**, 229 (1982).
19. M. Haelterman, S. Trillo, and S. Wabnitz, J. Opt. Soc. Am. B **11**, 446 (1994).
20. L. Del Bino, J. M. Silver, S. L. Stebbings, and P. Del'Haye, Sci. Rep. **7**, 43142 (2017).
21. M. T. M. Woodley, J. M. Silver, L. Hill, F. Copie, L. Del Bino, S. Zhang, G.-L. Oppo, and P. Del'Haye, Phys. Rev. A **98**, 053863 (2018).
22. B. Garbin, J. Fatome, G.-L. Oppo, M. Erkintalo, S. G. Murdoch, and S. Coen, Phys. Rev. Res. **2**, 023244/1 (2020).
23. M. T. M. Woodley, L. Hill, L. Del Bino, G.-L. Oppo, and P. Del'Haye, Phys. Rev. Lett. **126**, 043901 (2021).
24. E. Lucas, M. Karpov, H. Guo, M. L. Gorodetsky, and T. J. Kippenberg, Nat. Commun. **8**, 736 (2017).
25. A. U. Nielsen, B. Garbin, S. Coen, S. G. Murdoch, and M. Erkintalo, Phys. Rev. Lett. **123**, 013902/1 (2019).
26. K. Krupa, K. Nithyanandan, and P. Grelu, Optica **4**, 1239 (2017).